Published in final edited form as:
J Dent Res. 2011 January ; 90(1): 82–87. doi:10.1177/0022034510385241.

Biomimetic Analogs for Collagen Biomineralization

L. Gu[1,*], **Y. K. Kim**[2,*], **Y. Liu**[3,*], **H. Ryou**[4], **C. E. Wimmer**[5], **L. Dai**[6], **D. D. Arola**[4], **S. W. Looney**[5], **D. H. Pashley**[7], and **F. R. Tay**[7,8,†]

[1]Department of Operative Dentistry and Endodontics, Guanghua School of Stomatology, Sun Yat-sen University, Guangzhou, China

[2]Department of Conservative Dentistry, School of Dentistry, Kyungpook National University, Daegu, Korea

[3]Department of Stomatology, Tongji Hospital, Huazhong University of Science and Technology, Wuhan, China

[4]Laboratory of Advanced Materials and Processes, Mechanical Engineering Department, University of Maryland Baltimore County, Baltimore, MD, USA

[5]Department of Biostatistics, Medical College of Georgia, Augusta, GA, USA

[6]Department of Stomatology, The First Hospital of Wuhan, Wuhan, China

[7]Department of Oral Biology, School of Dentistry, Medical College of Georgia, Augusta, GA 30912-1129, USA

[8]Department of Endodontics, School of Dentistry, Medical College of Georgia, Augusta, GA 30912-1129, USA

Abstract

Inability of chemical phosphorylation of sodium trimetaphosphate to induce intrafibrillar mineralization of type I collagen may be due to the failure to incorporate a biomimetic analog to stabilize amorphous calcium phosphates (ACP) as nanoprecursors. This study investigated adsorption/desorption characteristics of hydrolyzed and pH-adjusted sodium trimetaphosphate (HPA-$Na_3P_3O_9$) to collagen. Based on those results, a 5-minute treatment time with 2.8 wt% HPA-$Na_3P_3O_9$ was used in a single-layer reconstituted collagen model to confirm that both the ACP-stabilization analog and matrix phosphoprotein analog must be present for intrafibrillar mineralization. The results of that model were further validated by complete remineralization of phosphoric-acid-etched dentin treated with the matrix phosphoprotein analog and lined with a remineralizing lining composite, and with the ACP-stabilization analog supplied in simulated body fluid. An understanding of the basic processes involved in intrafibrillar mineralization of reconstituted collagen fibrils facilitates the design of novel tissue engineering materials for hard tissue repair and regeneration.

Keywords

biomimetic; biomineralization; chemical phosphorylation; collagen; specific binding

†corresponding author, ftay@mcg.edu.
*authors contributing equally to this work;

A supplemental appendix to this article is published electronically only at http://jdr.sagepub.com/supplemental.

INTRODUCTION

Dentin matrix proteins possess important functions for controlling biomineralization (Zhang and Liu, 2007; George and Veis, 2008; Mahamid *et al*., 2008), such as stabilization of amorphous calcium phosphate (ACP) nano-precursors and controlling the oriented nucleation/growth of apatite within a collagen scaffold. These functions have to be recapitulated in biomimetic collagen mineralization (Xu *et al*., 2007; Gower, 2008; Tay and Pashley, 2008; Kim J *et al*., 2010).

Bioavailable polyphosphates appear to play an important role in the biomineralization of apatite (Omelon and Grynpas, 2008). Cyclic trimetaphosphate acts as a functional link in pre-biotic chemistry as a phosphorylation agent of bio-organic molecules (Ozawa *et al*., 2004). Sodium trimetaphosphate ($Na_3P_3O_9$) is a chemical phosphorylation reagent for food proteins (Lee *et al*., 2005; Leone *et al*., 2008) and type I collagen (Gunasekaran, 2003). However, in the absence of an agent to stabilize ACP, the use of as a matrix phosphoprotein analog for collagen mineralization $Na_3P_3O_9$ resulted only in the large extrafibrillar mineral spheres deposited around the collagen matrix (Li and Chang, 2008). Similar large mineral spheres were formed in a collagen-apatite tissue engineering scheme (Lickorish *et al*., 2004). In the absence of intrafibrillar mineralization, these strategies cannot be regarded as true biomimetic processes (Bertassoni *et al*., 2009). When only a polycarboxylic acid stabilization analog was used, infiltration of ACP nano-precursors into collagen fibrils produced intrafibrillar mineralization that apparently lacked the hierarchical order of apatite arrangement in natural mineralized collagen (Deshpande and Beniash, 2008). Presumably, binding of polyphosphates to collagen provides a means for the oriented deposition of apatite crystallites.

Biomimetic analogs of dentin matrix phosphoproteins have been used in solution to remineralize incompletely-resin-infiltrated collagen matrices in hybrid layers created by dentin adhesives (Tay and Pashley, 2009). It is anticipated that binding of a matrix phosphoprotein analog directly to dentin collagen matrices will facilitate translation of this proof-of-concept biomimetic remineralization strategy into a clinically relevant delivery system. Thus, the first objective of the present study was to determine the optimal concentration for high-affinity binding of $Na_3P_3O_9$ to collagen within a clinically relevant time frame. The null hypothesis tested was that there are no differences between 5-minute and one-hour adsorption and desorption characteristics of the matrix phosphoprotein analog to collagen. The second objective was to test the applicability of those parameters in a single-layer reconstituted collagen mineralization model. The null hypothesis tested was that intrafibrillar mineralization does not proceed in an ordered manner when either the ACP-stabilization or matrix phosphoprotein analog is absent. The third objective was to validate the results of the single-layer reconstituted collagen model by remineralizing acid-etched dentin treated with the matrix phosphoprotein analog.

MATERIALS & METHODS

Adsorption/Desorption of Matrix Phosphoprotein Analog

Extracted non-carious human third molars (N = 150), obtained with approval from the MCG Human Assurance Committee, were used to prepare dentin powder with particle size < 38 μm (Nishitani *et al*., 2006). The dentin powder was treated at 4°C with 4 M guanidine HCl for initial non-collagenous protein (NCP) extraction, completely demineralized (see the Appendix) in 0.5 M EDTA, and re-treated with 4 M guanidine HCl for extraction of mineral-masked NCPs (Termine *et al*., 1980). All solutions contained protease inhibitors and were adjusted to pH 7.4. The collagen matrices were thoroughly water-rinsed and lyophilized.

We performed adsorption experiments by mixing 50 mg of demineralized collagen with 1 mL of hydrolyzed and pH-adjusted (HPA) $Na_3P_3O_9$ solution (Sigma-Aldrich, St. Louis, MO, USA) for 5 min or 1 hr. Twelve HPA-$Na_3P_3O_9$ concentrations (0–3 wt%) were used. Protein phosphorylation with $Na_3P_3O_9$ requires alkaline hydrolysis into its linear form, sodium polyphosphate (Matheis and Whitaker, 1984; Zhang *et al*., 2007). Thus, $Na_3P_3O_9$ was hydrolyzed at pH 12 for 5 hrs (Shen, 1966), followed by neutralization to pH 7.4 (Fig. 1A), with minimal reduction in its phosphorylation potential (Muhammad *et al*., 2000). Desorption was performed with 500 mM NaCl for 24 hrs (Singh *et al*., 1995). Experiments were conducted in triplicate. Reaction mixtures were centrifuged to retrieve the supernatants. We deduced the phosphate content in each supernatant using the ammonium molyb-date assay (Chen *et al*., 1956) by analyzing the colored phosphomolybdate complex at 820 nm. Unreacted ligand concentrations (R) in the supernatants were estimated by linear regression derived from known HPA-$Na_3P_3O_9$ concentrations. We calculated the amount of bound ligand by subtracting R from the corresponding initial concentration.

We used polynomial regression to model the relationship between HPA-$Na_3P_3O_9$ concentration and bound HPA-$Na_3P_3O_9$ after adsorption/desorption. We used simultaneous tests of linear contrasts with a Bonferroni adjustment to compare model coefficients between treatment groups. We estimated the maximum ligand uptake (B_{max}) using the fitted curve and used the interpolation method to estimate the concentration $K^{½}$ that would yield an uptake of $B_{max}/2$. Approximate 95% confidence limits for $K^{½}$ were obtained graphically and used to approximate its standard error. We used the Wald test to compare $K^{½}$ values between treatment groups. Two-tailed tests with a 0.05 significance level were used for all comparisons except where Bonferroni adjustment was applied.

We generated a Scatchard plot (Scatchard, 1949) of the adsorption data by plotting bound/free HPA-$Na_3P_3O_9$ as the ordinate and bound HPA-$Na_3P_3O_9$ as the abscissa. We used non-linear regression to obtain the best fit of the data-points for each time period. We used the tangent of each regressive curve at the intersection point with the ordinate to determine the free HPA-$Na_3P_3O_9$ concentration for “high affinity” binding among the heterogeneous binding modalities (Gandofi and Strom, 1981).

Fourier Transform–Infrared Spectroscopy (FT-IR)

We used a Nicolet 6700 FT-IR spectrophotometer (Thermo Scientific Inc., Waltham, MA, USA) with an attenuated total reflection (ATR) set-up to collect IR spectra from the demineralized collagen matrices (control) and after treatment with 2.8 wt% HPA-$Na_3P_3O_9$ For further examination of whether true chemical phosphorylation had occurred, the STMP-bound collagen was treated with 0.13 μg/mL alkaline phosphatase (Sigma-Aldrich) for 6 hrs at 37°C. After being rinsed 3x in deionized water, the enzyme-treated STMP-sorbed collagen matrices were re-subjected to FT-IR analysis. Spectra were collected between 4000 and 675 cm^{-1} at 4 cm^{-1} resolution by 32 scans. The data were normalized to the collagen amide I band (1715-1596 cm^{-1}) and superimposed for comparison.

Single-layer Collagen Mineralization Model

Formvar- and carbon-coated 400-mesh Ni grids (EMS, Hatfield, PA, USA) were placed over a 2 mg/mL collagen solution prepared from calf-skin-derived type I collagen (Sigma-Aldrich). We achieved self-assembly of collagen fibrils by neutralizing the collagen solution with ammonia vapor (7% v/v NH_4OH for 4 hrs). Collagen cross-linking was performed with 0.3 M 1-ethyl-3-(3-dimethylaminopropyl)-carbodiimide/0.06 MN- hydroxysuccinimide for 4 hrs. Fibrillar assembly was confirmed with uranyl-acetate-stained grids by transmission electron microscopy (TEM; JEM-1230, JEOL, Tokyo, Japan) at 110 kV.

Unstained grids containing cross-linked reconstituted colla- for 5 min, rinsed, gen were treated with 2.8 wt% HPA-$Na_3P_3O_9$ and air-dried. The grids were floated over a mineralization assembly composed of an experimental Portland-cement-based remineralizing composite and a phosphate-containing simulated body fluid (SBF). The light-polymerizable composite contained 45 wt% set Portland cement powder and 5 wt% silanized fumed silica dispersed in a hydrophilic dimethacrylate resin matrix (Kim YK *et al*., 2010). The latter permits the sustained release of Ca^{2+} and OH^- ions at pH > 9.25, which favors the formation of ACP (Meyer and Eanes, 1978). The SBF (Kokubo and Takadama, 2006) contained (in mM) 205.2 NaCl, 6.3 $NaHCO_3$, 4.5 KCl, 1.5 $K_2HPO_4{\cdot}3H_2O$, 2.25 $MgCl_2{\cdot}6H_2O$, 3.75 $CaCl_2$, and 0.75 Na_2SO_4, with 3.08 NaN_3 to prevent bacterial growth. Polyacrylic acid (PAA; 0.28 mM, Mw = 1800, Sigma-Aldrich) was included in the SBF as the ACP-stabilization analog (Tay and Pashley, 2008). The ACP-stabilization analog negative control consisted of cross-linked collagen treated with HPA-$Na_3P_3O_9$, but without PAA in the SBF. The matrix phosphoprotein analog negative control consisted of cross-linked collagen with- treatment, but with PAA in the SBF. The grids out HPA-$Na_3P_3O_9$ were incubated for 4/24 hrs in a 100% humidity chamber. After retrieval, each grid was dipped in and out of deionized water to remove loose precipitates and was examined unstained. Selected area electron diffractions (SAEDs) were performed with centered dark-field imaging.

Remineralization of Acid-etched Dentin

We used non-carious third molars obtained under the same Human Assurance protocol (N = 6) to create mid-coronal dentin surfaces, using an Isomet saw (Buehler, Lake Bluff, IL, USA) under water cooling. Each surface was polished with 600-grit silicon carbide paper under running water, and etched with 32% H_3PO_4 gel for 15 sec to create a 5- to 8-μm-thick layer of completely demineralized collagen matrix over a mineralized dentin base. After undergoing water-rinsing, the collagen matrix was treated with 2.8 wt% HPA-$Na_3P_3O_9$ for 5 min, rinsed with deionized water, covered with the Portland-cement-based lining composite, and light-cured in two 1-mm-thick increments for 40 sec each at 600 mW/cm^2.

Each composite-lined dentin specimen was immersed in 15 mL of PAA-containing SBF, which was replaced monthly. Specimens were retrieved after 1–4 mos. Each specimen was sectioned occlusogingivally to obtain a 0.9-mm-thick slab. Exposed composite-dentin surfaces of intact specimens were protected with nail varnish for continuous remineralization prior to being re-sectioned in subsequent mos. The slabs were processed for TEM (Tay and Pashley, 2008). Non-demineralized sections were examined unstained at 110 kV.

RESULTS

Quadratic models provided an excellent fit for all adsorption and desorption isotherms (Fig. 1B) with highly significant omnibus F-tests ($p < 0.0001$) and adjusted R^2 values (> 0.994) for each model. Simultaneous tests of linear contrasts with a Bonferroni-adjusted significance level of 0.05/2 = 0.025 comparing the coefficients of the 2 adsorption quadratic models yielded significant differences between the 2 models in both quadratic [$F(1,16) = 13.12$; $p = 0.002$] and linear terms [$F(1,16) = 16.71$; $p < 0.001$]. In contrast, no significant difference was observed for the 2 desorption models at the 0.025 Bonferroni-adjusted significance level: $F(1,16) = 0.02$, $p = 0.888$; and $F(1,16) = 0.04$, $p = 0.851$, for the quadratic and linear terms, respectively. Estimated $K^{½}$ values for the 4 isotherms are shown in the Appendix Table. The transformed adsorption data yielded nonlinear Scatchard plots with adjusted R^2 values > 0.960 for each exponential regression model (Fig. 1C). The derivative of each exponential function at its intersection with the ordinate yielded “high-affinity” constants of 0.356 and 0.501, respectively, for the 5-minute and one-hour models. The

ligand concentration for “high-affinity” binding was approximated to be 2.81 wt% for the 5-minute and 2.0 wt% for the one-hour interaction. The more clinically realistic 5-minute treatment time was used for subsequent experiments.

Banding was observed from negative-stained reconstituted fibrils that were greater than 50 nm in diameter (Fig. 2A). For the ACP-stabilization analog negative control, 0.5- to 2-μm-diameter ACP microspheres (Tay *et al*., 2007) were present around unmineralized collagen fibrils after 24 hrs (Fig. 2B). For the matrix phosphoprotein analog negative control, 20- to 50-nm-diameter ACP nanospheres were observed at 4 hrs (Fig. 2C). These amorphous phases were initially completely devoid of needle-shaped crystallites (Appendix Fig. 1). Extrafibrillar mineral deposition and sparse intrafibrillar mineralization in the form of electron-dense microfibrillar strands were observed after 24 hrs. Banding was absent within the partially mineralized fibrils (Fig. 2D).

Infrared spectra of the demineralized collagen matrices before and after treatment with HPA-$Na_3P_3O_9$ are shown in Figs. 3A and 3B. Compared with the baseline, the intensities of the peaks related to the P=O and P–O–C stretching modes at 1080, 1030, 1010, and 976 cm^{-1} increased after chemical phosphorylation with sodium trimetaphosphate. These peaks returned to their original intensities after alkaline phosphatase treatment.

Reconstituted collagen treated with 2.8 wt% HPA-$Na_3P_3O_9$ for 5 min exhibited a gradient of mineralization after 24 hrs of immersion in the PAA-containing mineralization medium (not shown). Periodicity was observed in unstained fibrils, although intrafibrillar minerals appeared to be amorphous (Fig. 3C). Intrafibrillar apatite nanocrystals were present in the more highly mineralized fibrils (Fig. 3D). The nanocrystals were confirmed to be apatite by selected area electron diffraction (Fig. 3D), with a biologic apatite standard derived from non-demineralized dentin (Appendix Fig. 2).

Remineralization was not apparent after the 2.8 wt% HPA-$Na_3P_3O_9$-treated acid-etched dentin was immersed in the PAA-containing mineralization medium for 1 mo (Fig. 4A). A high-magnification view of the Portland-cement-containing lining composite is shown in Fig. 4B. Partial remineralization occurred at 2 mos (not shown). Complete remineralization of the acid-etched dentin could be observed in 90% of the specimens after 3–4 mos (Fig. 4C), with evidence of intrafibrillar mineralization within the collagen matrix (Fig. 4D).

DISCUSSION

Since there was a significant difference between the 5-minute and one-hour adsorption characteristics of HPA-$Na_3P_3O_9$ to collagen, the first null hypothesis has to be rejected. This difference may be due to the slow adsorption kinetics of HPA-$Na_3P_3O_9$, since the latter has to diffuse through the multiple intrafibrillar water compartments (Cameron *et al*., 2007) of a collagen fibril before it can phosphorylate the collagen molecules. Although there was significantly more adsorption of the HPA-$Na_3P_3O_9$ to collagen after 1 hr, the 5-minute time-point was chosen for the subsequent parts of the study, since it was more clinically realistic. We compensated for this time-factor by using a higher concentration of HPA-$Na_3P_3O_9$, as approximated from the Scatchard plots (2.8 wt% instead of 2.0 wt%). Based on the nonlinear Scatchard plots alone, one cannot establish whether the “high affinity” binding among the heterogeneous populations of binding sites was caused by chemical phosphorylation of the templating analog. However, the observation that part of HPA-$Na_3P_3O_9$ remained firmly bound to the collagen matrix after desorption with a salt solution of even higher ionic strength than the SBF used in the subsequent parts of the study clearly indicated that that “high affinity” binding was attributed to irreversible (covalent) binding. This was further confirmed by Fourier-transform infrared spectroscopy.

In the absence of a stabilization analog, the ACP microspheres were too large to infiltrate the internal compartments of collagen fibrils, and hence intrafibrillar mineralization did not occur. Although the PAA-stabilized ACP nanospheres could infiltrate the fibrils and resulted in intrafibrillar mineralization, collagen banding was not apparent in the partially mineralized fibrils. Conversely, in the presence of both analogs, banding reappeared in the initially light-mineralized fibrils. Since the fibrils were unstained, and no heavy metals were used in the mineralization procedure that could have led to negative staining, the highly regular periodicity within those banded fibrils could be attributed only to the hierarchical arrangement of electron-dense intrafibrillar mineral phases in the presence of the bound matrix phosphoprotein analog.

Cross-banding was difficult to be discerned with the more highly mineralized fibrils, since they were examined in a three-dimensional manner without being sectioned. Nevertheless, progressive dehydration of the fibrils by apatite replacement (Magne *et al*., 2001; Wehrli and Fernández-Seara, 2007) of the loosely bound water from the internal compartments of the fibrils (Cameron *et al*., 2007) resulted in the appearance of surface irregularities on those fibrillar surfaces, when compared with the less highly mineralized fibrils. Although those elevations were irregular, periodic surface elevations corresponding to internal banding periodicities could be identified from moderately mineralized fibrils with minerals still in the amorphous phase (Appendix Fig. 3). Thus, the second null hypothesis, that intrafibrillar mineralization does not proceed in an ordered manner when either the ACP-stabilization or matrix phosphoprotein analog is absent, has to be accepted. The single-layer collagen mineralization model has immediate application as a rapid screening tool for potential biomimetic analogs for collagen mineralization. Moreover, the technique may be modified for creating intrafibrillarly mineralized collagen coatings on the surfaces of orthopedic and dental implants as a more bio-compatible alternative to the use of hydroxyapatite coatings (de Jonge *et al*., 2010).

Since appropriate controls were already used in the single-layer reconstituted collagen model, the third part of the study was performed without additional controls, since its purpose was to validate the results of the reconstituted collagen model by remineralizing acid-etched dentin treated with the matrix phosphoprotein analog. In our previous biomimetic mineralization protocol, both the ACP-stabilization and matrix phosphoprotein analogs were supplied in solution with continuous replenishment. Delivery of calcium and hydroxyl ions was achieved by lateral diffusion from a set Portland cement block (Tay and Pashley, 2008, 2009). In the present study, we have translated our biomimetic strategy from its initial proof-of-concept design by binding the matrix phosphoprotein analog directly to the collagen matrix, without further replenishment. An experimental Portland-cement-based lining composite was also applied directly to the acid-etched collagen surface to simulate the clinical scenario of applying a liner over caries-affected dentin. With the encouraging results obtained from the validation part of the present study, the next step will involve designs for *in situ* delivery of the ACP-stabilization analog. This will facilitate translation of the proof-of-concept biomimetic strategy into a clinically relevant delivery system for remineralizing incompletely-resin-infiltrated dentin hybrid layers as well as caries-affected dentin.

Supplementary Material

Refer to Web version on PubMed Central for supplementary material.

Acknowledgments

This work was supported by grant R21 DE019213 from NIDCR (PI. Franklin Tay). We thank Michelle Barnes for secretarial support and Thomas Bryan for technical support.

References

Bertassoni LE, Habelitz S, Kinney JH, Marshall SJ, Marshall GW Jr. Biomechanical perspective on the remineralization of dentin. Caries Res. 2009; 43:70–77. [PubMed: 19208991]

Cameron IL, Short NJ, Fullerton GD. Verification of simple hydration/dehydration methods to characterize multiple water compartments on tendon type 1 collagen. Cell Biol Int. 2007; 31:531–539. [PubMed: 17363297]

Chen PS, Toribara TY, Warner H. Microdetermination of phosphorus. Anal Chem. 1956; 28:1756–1758.

de Jonge LT, Leeuwenburgh SC, van den Beucken JJ, te Riet J, Daamen WF, Wolke JG, et al. The osteogenic effect of electrosprayed nanoscale collagen/calcium phosphate coatings on titanium. Biomaterials. 2010; 31:2461–2469. [PubMed: 20022365]

Deshpande AS, Beniash E. Bio-inspired synthesis of mineralized collagen fibrils. Cryst Growth Des. 2008; 8:3084–3090.

Gandolfi A, Strom R. Analysis of binding curves in multivalent antigen-heterogeneous antibody systems. J Theor Biol. 1981; 92:57–84. [PubMed: 6173544]

George A, Veis A. Phosphorylated proteins and control over apatite nucleation, crystal growth and inhibition. Chem Rev. 2008; 108:4670–4693. [PubMed: 18831570]

Gower LB. Biomimetic model systems for investigating the amorphous precursor pathway and its role in biomineralization. Chem Rev. 2008; 108:4551–4627. [PubMed: 19006398]

Gunasekaran, S. Purifying type I collagen using two papain treatments and reducing and delipidation agents. United States Patent No. 6,548,077. 2003. Available at http://www.freepatentsonline.com/6548077.html

Kim J, Arola DD, Gu L, Kim YK, Mai S, Liu Y, et al. Functional biomimetic analogs help remineralize apatite-depleted demineralized resin-infiltrated dentin via a bottom-up approach. Acta Biomater. 2010; 6:2740–2750. [PubMed: 20045745]

Kim YK, Gu L-S, Bryan TE, Kim JR, Chen L, Liu Y, et al. Mineralization of reconstituted collagen using polyvinylphosphonic acid/polyacrylic acid templating matrix protein analogues in the presence of calcium, phosphate and hydroxyl ions. Biomaterials. 2010; 31:6618–6627. [PubMed: 20621767]

Kokubo T, Takadama H. How useful is SBF in predicting *in vivo* bone bioactivity? Biomaterials. 2006; 27:2907–2915. [PubMed: 16448693]

Lee SH, Yang JI, Hong SM, Hahm DH, Lee SY, Kim IH, et al. Phosphorylation of peptides derived from isolated soybean protein: effects on calcium binding, solubility and influx into Caco-2 cells. Biofactors. 2005; 23:121–128. [PubMed: 16410634]

Leone G, Torricelli P, Giardino R, Barbucci R. New phosphorylated derivatives of carboxymethylcellulose with osteogenic activity. Polym Adv Technol. 2008; 19:824–830.

Li X, Chang J. Preparation of bone-like apatite-collagen nanocomposites by a biomimetic process with phosphorylated collagen. J Biomed Mater Res A. 2008; 85:293–300. [PubMed: 17688292]

Lickorish D, Ramshaw JA, Werkmeister JA, Glattauer V, Howlett CR. Collagen-hydroxyapatite composite prepared by biomimetic process. J Biomed Mater Res A. 2004; 68:19–27. [PubMed: 14661245]

Magne D, Weiss P, Bouler JM, Laboux O, Daculsi G. Study of the maturation of the organic (type I collagen) and mineral (nonstoichiometric apatite) constituents of a calcified tissue (dentin) as a function of location: a Fourier transform infrared microspectroscopic investigation. J Bone Miner Res. 2001; 16:750–757. [PubMed: 11316003]

Mahamid J, Sharir A, Addadi L, Weiner S. Amorphous calcium phosphate is a major component of the forming fin bones of zebrafish: indications for an amorphous precursor phase. Proc Natl Acad Sci USA. 2008; 105:12748–12753. [PubMed: 18753619]

Matheis G, Whitaker JR. Chemical phosphorylation of food proteins: an overview and a prospectus. J Agric Food Chem. 1984; 32:699–705.

Meyer JL, Eanes ED. A thermodynamic analysis of the secondary transition in the spontaneous precipitation of calcium phosphate. Calcif Tissue Res. 1978; 25:209–216. [PubMed: 30523]

Muhammad K, Hussin F, Man YC, Gjazali HM, Kennedy JF. Effect of pH on phosphorylation of sago starch. Carbohydr Polym. 2000; 42:85–90.

Nishitani Y, Yoshiyama M, Wadgaonkar B, Breschi L, Mannello F, Mazzoni A, et al. Activation of gelatinolytic/collagenolytic activity in dentin by self-etching adhesives. Eur J Oral Sci. 2006; 114:160–166. [PubMed: 16630309]

Omelon SJ, Grynpas MD. Relationships between polyphosphate chemistry, biochemistry and apatite biomineralization. Chem Rev. 2008; 108:4694–4715. [PubMed: 18975924]

Ozawa K, Nemoto A, Imai E, Honda H, Hatori K, Matsuno K. Phosphorylation of nucleotide molecules in hydrothermal environments. Orig Life Evol Biosph. 2004; 34:465–471. [PubMed: 15573497]

Scatchard G. The attraction of proteins for small molecules and ions. Ann NY Acad Sci. 1949; 51:660–672.

Shen CY. Alkaline hydrolysis of sodium trimetaphosphate in concentrated solutions and its role in built detergents. Ind Eng Chem Prod Res Dev. 1966; 5:272–276.

Singh MP, Lumpkin JA, Rosenblatt J. Effect of electrostatic interactions on polylysine release rates from collagen matrices and comparison with model predictions. J Control Release. 1995; 35:165–179.

Tay FR, Pashley DH. Guided tissue remineralisation of partially demineralised human dentine. Biomaterials. 2008; 29:1127–1137. [PubMed: 18022228]

Tay FR, Pashley DH. Biomimetic remineralization of resin-bonded acid-etched dentin. J Dent Res. 2009; 88:719–724. [PubMed: 19734458]

Tay FR, Pashley DH, Rueggeberg FA, Loushine RJ, Weller RN. Calcium phosphate phase transformation produced by the interaction of the Portland cement component of white mineral trioxide aggregate with a phosphate-containing fluid. J Endod. 2007; 33:1347–1351. [PubMed: 17963961]

Termine JD, Belcourt AB, Christner PJ, Conn KM, Nylen MU. Properties of dissociatively extracted fetal tooth matrix proteins. J Biol Chem. 1980; 255:9760–9768. [PubMed: 7430099]

Wehrli FW, Fernández-Seara MA. Nuclear magnetic resonance studies of bone water. Ann Biomed Eng. 2005; 33:79–86. [PubMed: 15709708]

Xu AW, Ma YR, Cölfen H. Biomimetic mineralization. J Mater Chem. 2007; 17:415–449.

Zhang K, Li Y, Ren Y. Research on the phosphorylation of soy protein isolate with sodium tripolyphosphate. J Food Eng. 2007; 79:1233–1237.

Zhang TH, Liu XY. How does a transient amorphous precursor template crystallization. J Am Chem Soc. 2007; 129:13520–13526. [PubMed: 17929918]

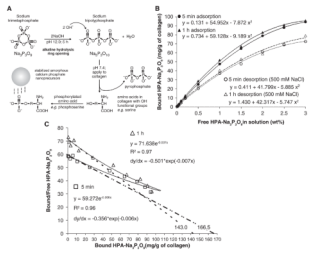

Figure 1.

Adsorption and desorption characteristics of sodium trimetaphosphate. **(A)** Sodium trimetaphosphate ($Na_3P_3O_9$) was used for introducing a matrix phosphoprotein analog to collagen. Ring opening was achieved by alkaline hydrolysis at pH 12 for 5 hrs to produce sodium tripolyphosphate ($Na_5P_3O_{10}$). The pH of $Na_5P_3O_{10}$ was adjusted to 7.4 to retain its phosphorylation potential. The phosphorylated amino acids on the collagen molecules function as templates for attracting polyacrylic-acid-stabilized amorphous calcium phosphate nanoprecursors. (**B)** Adsorption and desorption isotherms of different ligand concentrations (hydrolyzed and pH-adjusted $Na_3P_3O_9$, hereafter referred to as HAP-$Na_3P_3O_9$) to demineralized collagen matrices for 5 min and 1 hr at 37°C. Each point represents the mean of triplicate assays. Twelve different HAP-$Na_3P_3O_9$ concentrations (wt %) were used: 0, 0.01, 0.02, 0.05, 0.1, 0.2, 0.5, 1.0, 1.5, 2.0, 2.5, and 3. **(C)** Corresponding Scatchard plot transformed from the 5-minute (open squares) and one-hour (open triangles) adsorption data in (A) yielded nonlinear plots (solid lines) that are suggestive of several populations of binding sites in the collagen matrix, with different ligand affinities. The tangent (dotted lines) of each regressive curve at the point of intersection of the curve with the Y-axis was extrapolated to determine the optimal free ligand concentration for irreversible binding.

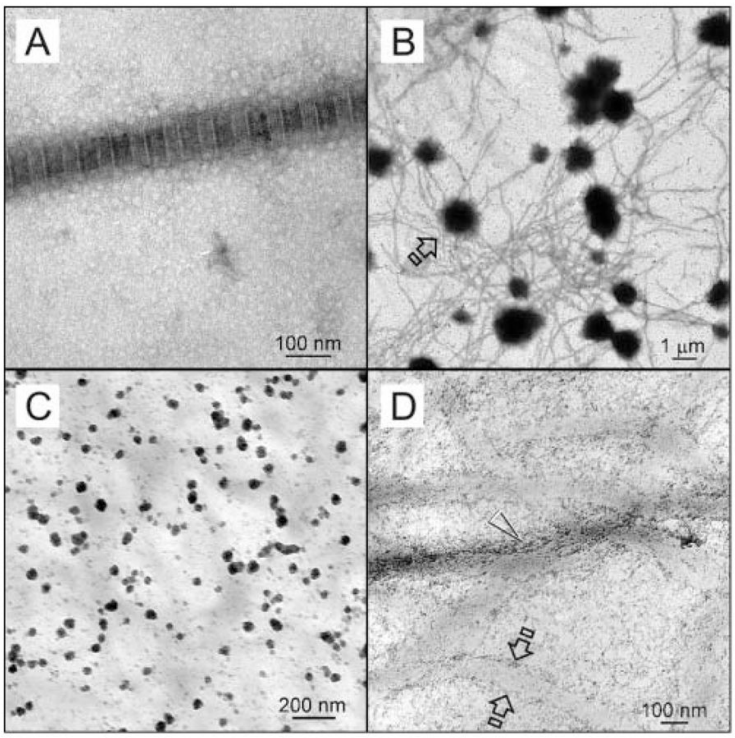

Figure 2.

TEM images of collagen fibrils before mineralization and those obtained from controls. **(A)** Negative-stained, cross-linked reconstituted collagen fibril with approximately 76 nm periodicity. (**B)** Unstained image of the sequestration analog negative control. Electron-dense microspheres (open arrow; *ca*. 0.5–2 μm) were formed around unmineralized collagen fibrils after they were phosphorylated with HPA-$Na_3P_3O_9$. However, no intrafibrillar mineralization was observed after 24 hrs. (**C)** Unstained image of the matrix phosphoprotein analog negative control retrieved after 4 hrs, showing formation of electron-dense nanospheres (arrow; *ca*. 20–50 nm) in the vicinity of the unmineralized, non-phosphorylated collagen matrix when polyacrylic acid was included as an ACP-stabilization analog in the mineralization medium. (**D)** Unstained image of the matrix phosphoprotein analog negative control retrieved after 24 hrs. Minerals were formed along fibril surfaces (between open arrows). Intrafibrillar mineralization was seen as electron-dense microfibrillar strands, but no banding could be identified.

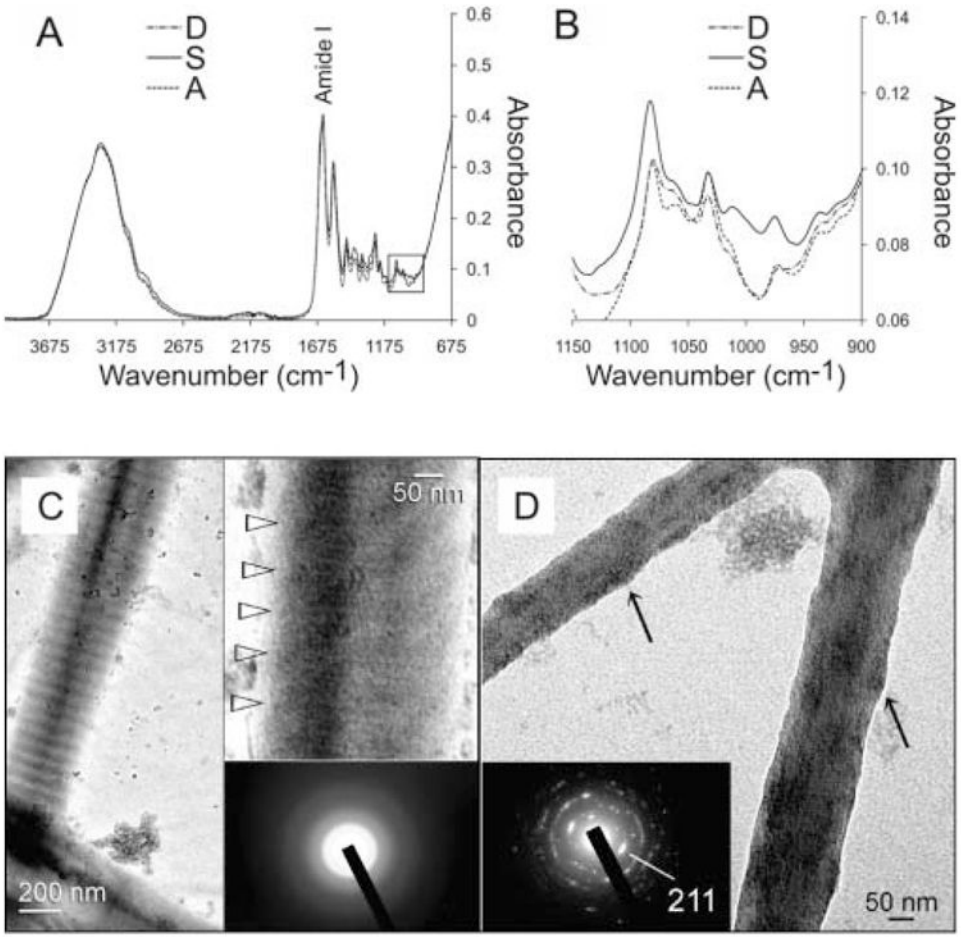

Figure 3.

Collagen mineralization in the presence of sodium trimetaphosphate. **(A)** Infrared spectra (4000-675 cm^{-1}) of demineralized collagen matrices (spectrum D), followed by chemical phosphorylation with 2.8 wt% hydrolyzed and pH-adjusted sodium trimetaphosphate (spectrum S) and dephosphorylation with alkaline phosphatase (spectrum A). (**B)** High magnification of the 3 spectra (1150-900 cm^{-1}) from the region depicted by the square box in (A). (**C)** Unstained images of reconstituted collagen phosphorylated with HPA-$Na_3P_3O_9$ after 24 hrs of immersion in the polyacrylic-acid-containing mineralization medium. A banded fibril showing electron-dense mineral phases along the fibril surface (arrow). Top inset: High-magnification view of the periodicity (open arrowheads) within the fibril, which is suggestive of an ordered deposition of mineral phases. Bottom inset: Selected area electron diffraction (SAED) showing that the intrafibrillar minerals were amorphous at this stage. (**D)** More highly mineralized fibrils from the periphery of the grid space showing intrafibrillar nanocrystals. These fibrils appear shrunken, since loosely bound water within the internal compartments of the fibrils was replaced by minerals, resulting in elevations along the fibrillar surfaces (arrows). Inset: SAED of the intrafibrillar minerals showing arc-shaped concentric rings characteristic of apatite.

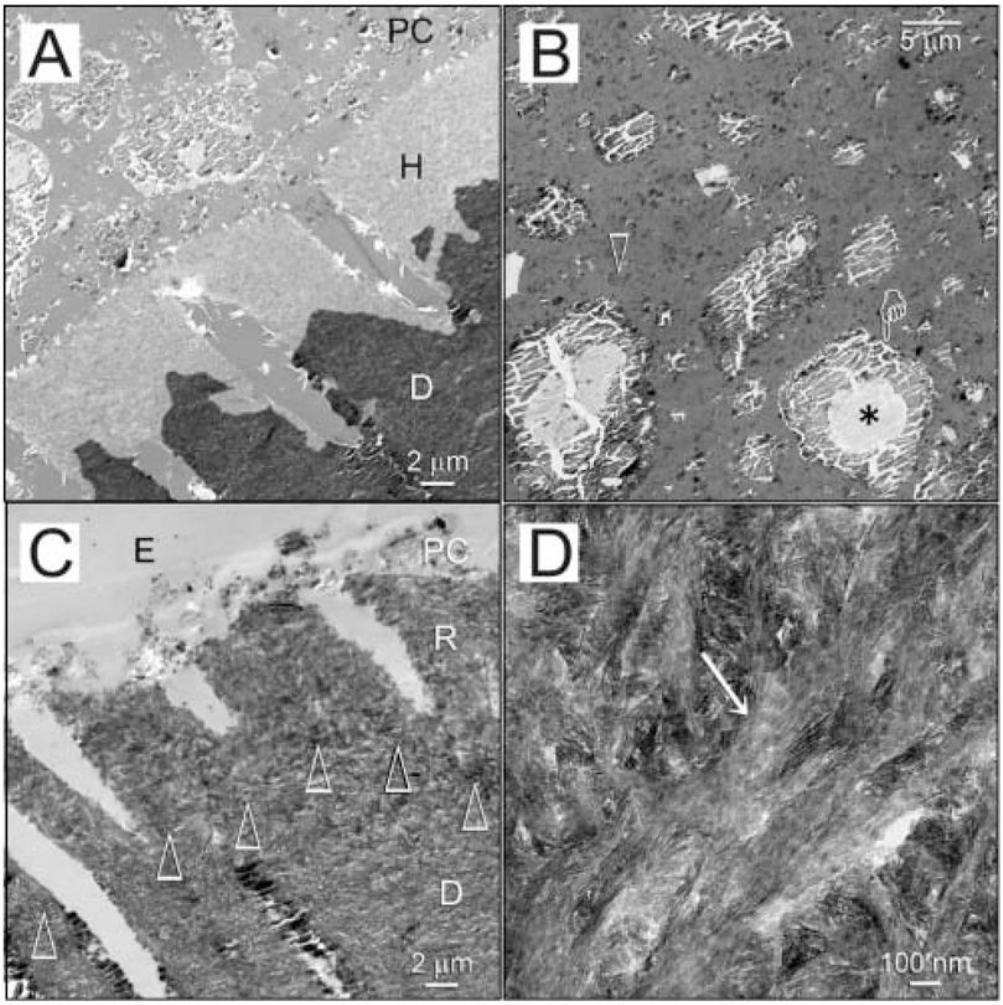

Figure 4.

Biomimetic remineralization of acid-etched dentin with sodium trimetaphosphate. **(A)** Unstained image of acid-etched dentin (AE) phosphorylated with HPA-$Na_3P_3O_9$ for 5 min and capped with a Portland-cement-containing composite (PC). No remineralization was seen after 1 mo of immersion in the sequestration analog-containing mineralization medium. D: mineralized dentin. (**B)** The composite contains set Portland cement and silanized silica (open arrow) within its resin matrix. The Portland cement particles contain a cement core (asterisk) surrounded by calcium silicate hydrate (pointer). (**C)** Unstained image of the completely remineralized layer (R) of acid-etched dentin after 3–4 mos of biomimetic remineralization. The original demineralization front is demarcated by open arrowheads. The composite (PC) had dislodged, leaving a thin layer embedded by laboratory epoxy resin (E). D: mineralized dentin. (**D)** Intrafibrillar mineralization (open arrowhead) within the remineralized layer.